The Ocular Surface 36 (2025) 224–236

Contents lists available at ScienceDirect

The Ocular Surface

journal homepage: www.elsevier.com/locate/jtos

Development and optimization of an *ex vivo* model of corneal epithelium damage with 1-heptanol: Investigating the influence of donor clinical parameters and MSC-sEV treatment on healing capacity

Filippo Bonelli [a,*,1], Seyedmohammad Moosavizadeh [b,c,1], Elisa Fasolo [a], Alessia Di Nella [d], Vanessa Barbaro [a], Ilaria Zorzi [a], Mauro Krampera [d], Jana D'Amato Tóthová [e], Diego Ponzin [a], Thomas Ritter [b,c], Stefano Ferrari [a], Umberto Rodella [a,e]

[a] *Fondazione Banca Degli Occhi Del Veneto ETS, Venice, Italy*
[b] *Regenerative Medicine Institute (REMEDI), School of Medicine, College of Medicine Nursing and Health Science, University of Galway, Galway, Ireland*
[c] *SFI Research Centre for Medical Devices (Curam), University of Galway, Galway, Ireland*
[d] *Hematology and Bone Marrow Transplant Unit, Section of Biomedicine of Innovation, Department of Engineering for Innovative Medicine (DIMI), University of Verona, Italy*
[e] *Research and Development, AL.CHI.MI.A. S.R.L, Ponte San Nicolò, Italy*

ARTICLE INFO

Keywords:
1-Heptanol
Corneal epithelium
Epithelial Re
Human cornea
Mesenchymal stromal cells
Small extracellular vesicles
Wound/healing

ABSTRACT

Purpose: To develop and characterize a reproducible human corneal epithelial wound-healing model using 1-heptanol, and to investigate the healing potential of Bone Marrow-derived Mesenchymal Stromal Cell small Extracellular Vesicles (MSC-sEV) and the influence of donor characteristics on epithelial healing.
Methods: Eighty-eight (n = 88) human corneoscleral tissues unsuitable for transplantation were employed. Corneal epithelial damage was induced with 1-heptanol and monitored every 24 h up to 96 h using fluorescein and trypan blue staining. Histological assessment was performed on untreated and damaged tissues. Damaged areas were measured with FIJI software, and healing rates were calculated. MSC-sEV were isolated with size exclusion chromatography and characterized for their size, morphology and biomarkers. Their impact on healing was assessed in both *in vitro* scratch assays on cultured human corneal epithelial cells and on *ex vivo* 1-heptanol-damaged corneas.
Results: Histological analysis revealed detached corneal epithelium in the central area, while other layers remained unaffected. Healing rate peaked at 48 h post-damage. Trypan blue and Fluorescein staining correlated and the former highlighted a higher initial healing rate than the latter. Diabetic and heart-beating brain-deceased donors showed impaired healing rates. MSC-sEV (79.8 nm, spherical bilayer, positive for TSG101, CD9, CD63, and CD81) significantly improved epithelial wound healing in both *in vitro* and *ex vivo* models.
Conclusion: 1-heptanol effectively induces reproducible corneal epithelial damage, and the *ex vivo* organ-cultured human cornea heals the epithelium within 96 h. Diabetes and donation from heart-beating brain-deceased donors reduce healing capacity. MSC-sEV boost epithelial repair in damaged corneas.

1. Introduction

The corneal epithelium constitutes the outermost layer of the cornea, serving as a protective barrier that shields the eye from mechanical, chemical, and biological insults [1]. Numerous factors can compromise corneal epithelial integrity, including mechanical trauma, chemical insults (e.g. alkali burns), corneal dryness, neurotrophic keratitis, post-surgical changes, and limbal stem cell deficiencies, thereby increasing the risk of microbial infections, ulceration, and impaired vision. Prompt repair of the epithelium is therefore crucial for maintaining ocular homeostasis in cases of epithelial damage.

Various *in vivo* models have been employed to study corneal epithelial repair. The predominant technique for wound healing assays involves mechanical scraping to induce epithelial denudation [2]. While

* Corresponding author. Fondazione Banca Degli Occhi Del Veneto ETS, Venice, Italy.
E-mail address: filippo.bonelli@maastrichtuniversity.nl (F. Bonelli).
[1] FB and SM contributed equally to this work.

https://doi.org/10.1016/j.jtos.2025.02.002
Received 26 July 2024; Received in revised form 20 January 2025; Accepted 3 February 2025
Available online 4 February 2025

effective, this method is subject to operator variability and can compromise the structural integrity of the underlying Bowman's layer, which is non-regenerative [1], as well as cause damage to the anterior keratocytes into the stroma [2]. Another widely used experimental method is the alkali burn technique, which is highly invasive and results in deep stromal damage [3].

Increasing evidence highlights the limited predictability of animal testing for novel therapies in humans, prompting the scientific community to develop alternatives [4,5]. Among these, 3D systems and human tissues currently demonstrate higher predictive potential [6].

1-Heptanol (chemical formula $CH_3(CH_2)_6OH$) is an alkyl alcohol characterized by a hydroxyl group replacing a hydrogen atom in one of the methyl groups. It is highly hydrophobic and exhibits limited diffusion in aqueous solutions. Its recognized cytotoxicity makes 1-heptanol an appealing method for wound healing studies, offering improved reproducibility and standardization compared to mechanical scraping. Additionally, this approach preserves the integrity of the epithelial basement membrane [7].

First described by Cintron et al. [7], the 1-heptanol method has been adopted in several *in vivo* [8–12] and *ex vivo* [13] animal models to study corneal epithelial healing capacity. The approach was later utilized by Ljubimov and collaborators in human corneas from diabetic donors [14–16].

Long-term complications of ocular injury/inflammation include reduced or complete loss of vision, corneal scarring and dry eye [17] which also impacts on quality of life and health care budgets. Gold standard has been topical corticosteroids, however there are serious side effects associated with its application [18]. Therefore, novel therapies have to be developed. Mesenchymal stromal cells (MSC) and more recently their secreted extracellular vesicles (MSC-EVs) have been shown to have significant therapeutic efficacy in many disease conditions [19–21]. MSC-EVs are lipid bilayer particles which are classified depending on their size, such as small EV (sEV) having a diameter smaller than 200 nm [22]. MSC-EVs and are known to mediate tissue repair, regeneration, anti-inflammation, and immunomodulation effects [23–26]. MSC-EVs address safety challenges [19,27] associated with cell therapies [19,20], and may serve as the foundation for future cell-free therapies in a range of clinical applications, including ocular diseases [19,27,28]. Noteworthy a clinical trial is investigating the effects of exosomes in dry eye disease (ID: NCT04213248). MSC-sEV have shown significant potential to enhance corneal epithelial repair through intercellular communication [29–32]. They carry proteins, lipids, and nucleic acids, mediating therapeutic effects by interacting with recipient cells via endocytosis, membrane fusion, or receptor interaction [33–35].

Given this background, the primary goal of the present study was to establish and optimize a novel and reproducible epithelial wound healing model based on *ex vivo* 1-heptanol damage of research-grade donated human corneas. Corneas under organ-culture conditions at 31 °C were included in the study as this kind of *ex vivo* preservation is designed to mimic *in vivo* conditions as closely as possible in order to sustain corneal metabolism. Fluorescein (FL) and Trypan Blue (TB) staining techniques were employed to monitor the healing progression over time.

After establishing the model, we investigated potential correlations between donor parameters and epithelial healing rates. This investigation was motivated by the recognition that donor parameters of human corneas influence epithelial physiology during preservation in eye banks [36–38].

The second main aim of this study was to evaluate the effect of small extracellular vesicles derived from human bone marrow mesenchymal stromal cells (MSC-sEV) on our newly developed corneal epithelial damage model. Overall, our study presents a new, animal-free model for studying corneal epithelial repair and suggests MSC-sEV as a promising tool to enhance this process.

2. Materials and methods

2.1. Human tissues

Human corneoscleral tissues (n = 88) deemed unsuitable for transplantation were obtained from the *Fondazione Banca degli Occhi del Veneto ETS* (FBOV, Venice, Italy) with the donor's next of kin consent for donation and in agreement with the Italian National Transplant Centre (Centro Nazionale Trapianti, Rome, Italy) guidelines. Donor data were obtained from FBOV database. The post-mortem time (i.e. the time interval -hours- between donor's decease and the cornea procurement) ranged from 1 to 25 h. All the tissues underwent slit lamp examination immediately after retrieval to evaluate potential tissue defects. The tissues used for this study were transported from the procurement site to the eye bank within 48 h in cold storage medium "Coldix" (FBOV, Venice, Italy) and organ-cultured in "Storagix" medium (FBOV, Venice, Italy) upon arrival to the eye bank in an incubator at 31 °C for a maximum period of 28 days, before the beginning of the experiments. Storagix contains Eagle's minimum essential medium (MEM) supplemented with foetal bovine serum (FBS) and antimicrobials. This study complied with the guidelines in the Declaration of Helsinki for research involving human tissues.

2.2. Chemical epithelial damage and healing monitoring

The method design described here is also visually described in Fig. 1. Before damage induction, corneas were evaluated with fluorescein (FL) and Trypan Blue (TB) to confirm epithelial integrity prior to the experiment. Evaluation with both FL and TB was chosen because of their two different mechanisms of tissue penetration. Indeed, FL identifies lack of barrier function and epithelial permeability due to paracellular entry [39], while TB stains dead cells as it penetrates through a damaged plasma membrane [40,41].

In order to detect corneal epithelial damage and irregularities, a sterile ophthalmic fluorescein (FL) strip (I-DEW FLO, Madhu Instruments Pvt. Ltd. Okhla industrial area, New Delhi, India) was immersed into sterile PBS and applied on the corneal epithelium for 1 min. Then corneas were rinsed by gentle immersion in PBS in order to remove FL excess. To visualize the FL fluorescence, corneas were placed on an UV transilluminator (Major Science Co., Ltd, Guoji Rd., Taoyuan Dist., Taoyuan City 33061, Taiwan).

To assess corneal epithelial viability, 400 μL of 0,25 % (w/V) Trypan blue (TB) solution (TB-S, AL.CHI.MI.A. S.R.L., Ponte San Nicolò, Italy) were pipetted into a concave, silicon cap. Corneas were then placed with the epithelium facing the bottom of the TB-filled container for 1 min. The tissues were then rinsed by gentle immersion in PBS to remove excess of dye and corneas were observed above a white background.

Only tissues exhibiting an intact and viable epithelium from both staining techniques were included in the study.

In order to perform a chemical damage at the corneal epithelium, sterile 6 mm diameter paper discs were soaked into 98 % 1-Heptanol (H2805, Sigma-Aldrich, St. Louis, MO, USA) and applied in the centre of the epithelium for 60 s. After that, the disc was removed and corneas were rinsed with PBS to remove excess of 1-heptanol. In order to monitor epithelial healing, pictures of both FL- and TB-stained corneas were captured immediately before as well as immediately after damage induction, and every 24 h up to 96 h, employing a mobile phone equipped with 12 MP, 3968x2976 pixel, aperture size F2.2 photo camera. At every time point each cornea was stained firstly with FL, then immediately with TB.

2.3. Healing rate calculation

In order to calculate the Healing Rate (HR) of human corneal epithelium following 1-heptanol damage, pictures at each time point, from both FL and TB staining, were processed using FIJI software

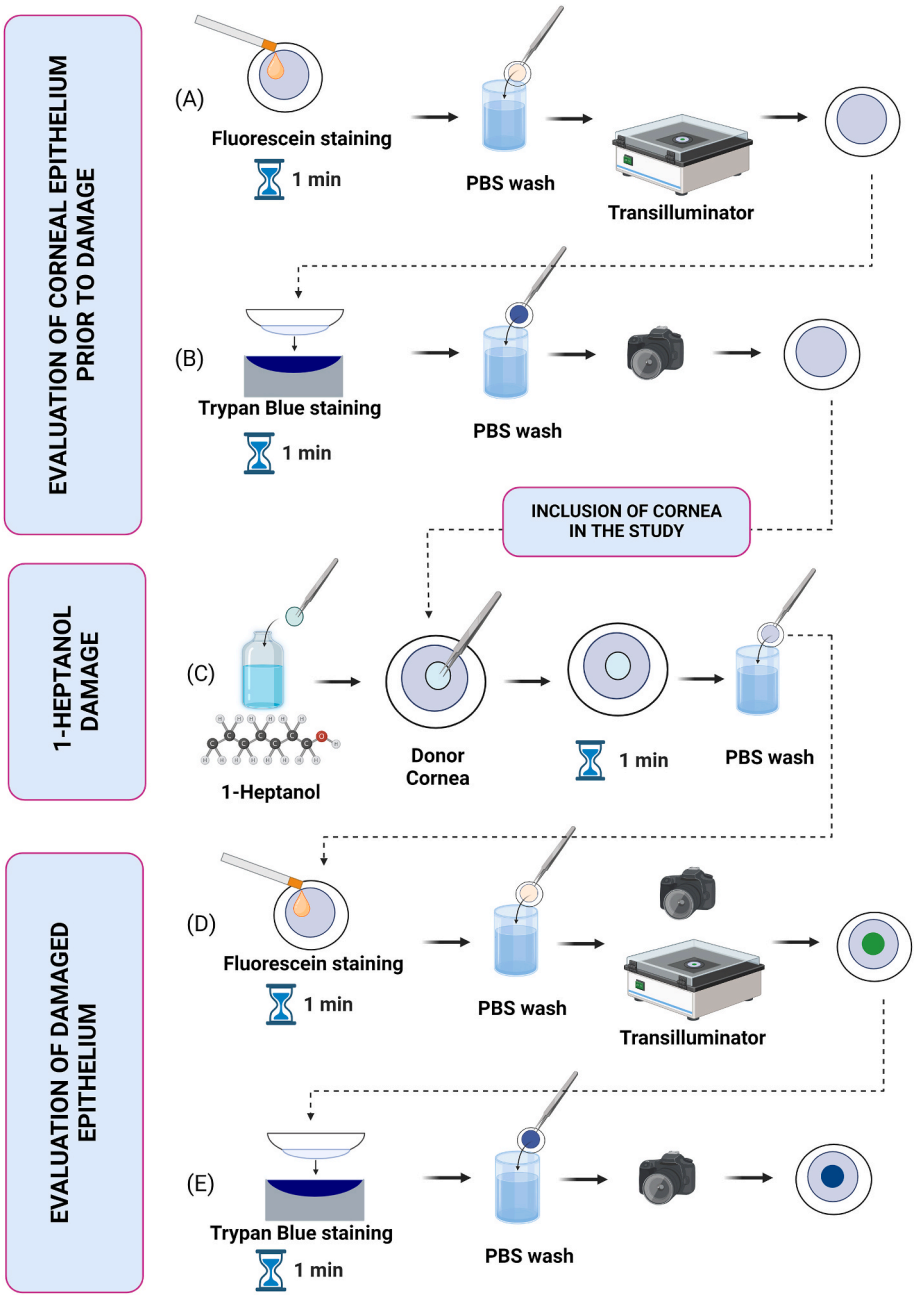

Fig. 1. Visual description of the chemical damage exerted at the corneal epithelium and damage visualization with Fluorescein (FL) and Trypan Blue (TB) staining. (A) A 6 mm diameter sterile paper disc is soaked into 1-heptanol. The soaked paper disc is then applied on the central area of corneal epithelium for 1 min in order to trigger chemical damage. The damage is kept confined to the application site as 1-heptanol displays low hydrophilicity and thus low dispersion in aqueous solution. The tissue is then rinsed by gentle immersion in PBS to remove 1-heptanol excess. (B) The corneal epithelium is stained with FL by application of PBS-soaked FL strips on the epithelium. After 1 min, the cornea is rinsed in PBS to remove FL excess. FL-stained epithelial areas can be observed under UV transilluminator light, revealing damaged epithelium. A picture is acquired for data analysis. (C) TB staining is performed on corneal epithelium for 1 min, then the cornea is rinsed in PBS to remove TB excess. TB-stained epithelial areas can be observed by the naked eye, revealing non-viable epithelial areas. A picture is acquired for data analysis. Created with biorender.com. (For interpretation of the references to colour in this figure legend, the reader is referred to the Web version of this article.)

(Supplementary Fig. 1) [42]. Determination of area and perimeter of the wound were obtained by manually drawing a Region Of Interest (ROI) on the FL- (or TB-) stained epithelial perimeter, eventually obtaining values in pixels by FIJI quantification. The precision (repeatability) of manual drawing of ROIs was assessed by calculating coefficient of variation (CV%) of eight repeated ROIs into the same image, with CV% < 2 % being considered acceptable. Bias introduced by interoperator variability in the estimation of FL- and TB-stained epithelial areas (expressed in mm^2) was assessed using the Bland-Altman method [43, 44] provided by SimplyAgree and blandr modules in jamovi computer software (Version 2.5, The jamovi project, 2024) on values obtained by two blinded operators performing the analytical procedure on the same, randomly chosen images ($n = 20$). The limits of agreement (LoA) were defined as the mean difference between parameters $\pm$ 1.96 $\times$ SD. The inner diameter of the 35-mm Petri dish containing the cornea was calculated as internal calibration reference. This allowed the conversion of data from pixels into square millimetres (mm^2), through a proportion (Table 1, Equation (1)). The HR at each time point was calculated as described by Vidal and colleagues [45] (Table 1, Equation (2)) and the average HR (HR_{avg}) was calculated as the arithmetical average of all HRs

Table 1
Equations employed to calculate Healing Rates (HR) of human corneal epithelia after damage with 1-heptanol on images taken after FL and TB stainings.

Equation 1	$D[px] : A[px] = D : A$ $D = \frac{D[px]*A}{A[px]} = \frac{D[px]*962.11\ mm^2}{\pi\left(\frac{d[px]}{2}\right)^2}$ *Where:* *D: Damaged area, expressed in* mm^2 *D[px]: Damaged area, expressed in pixels* *A: Total Petri dish area, corresponding to:* $\pi(35mm/2)^2 = 962.11\ mm^2$ *A[px]: Total Petri dish area, expressed in pixels d[px]: Petri dish diameter, expressed in pixels*
Equation 2	$HR_{(t_x:t_y)} = \frac{\Delta Damage\ area\ between\ t_x\ and\ t_y}{average\ perimeter\ of\ damage\ between\ t_x\ and\ t_y * \Delta t} = \frac{\frac{D_{t_x} - D_{t_y}}{(P_{t_x} + P_{t_y})}}{2} * (t_x - t_y)$ *Where:* $HR_{(tx:ty)}$*: Healing Rate between time point "x" and time point "y", expressed in mm/day* D_{tx}*: Damaged area at time point "x", expressed in* mm^2 D_{ty}*: Damaged area at time point "y", expressed in* mm^2 P_{tx}*: Perimeter of damaged area at time point "x", expressed in mm* P_{ty}*: Perimeter of damaged area at time point "y", expressed in mm* t_x*: time point "x", expressed in day* t_y*: time point "y", expressed in day*
Equation 3	$HR_{avg} = \frac{HR_{(t_w:t_1)} + HR_{(t_1:t_2)} + HR_{(t_2:t_3)} + HR_{(t_3:t_4)}}{4}$ *Where:* HR_{avg}*: Average Healing Rate during the wound/healing kinetics, expressed in mm/day* t_w*: initial wounding time point* $t_{1,2,3,4}$*: day 1, 2, 3 and 4 post wounding* $HR_{(tw:t1)}$*: Healing Rate between wounding time point and day 1 post wounding, expressed in mm/day* $HR_{(t1:t2)}$*: Healing Rate between day 1 and day 2 post wounding, expressed in mm/day* $HR_{(t2:t3)}$*: Healing Rate between day 2 and day 3 post wounding, expressed in mm/day* $HR_{(t3:t4)}$*: Healing Rate between day 2 and day 3 post wounding, expressed in mm/day*

calculated at every time point (Table 1, Equation (3)).

For each tissue HR was calculated separately on images following FL (HR^{FL}) and as well as TB (HR^{TB}) staining.

2.4. Analysis of healing rate in donor subgroups

To determine whether specific donor characteristics can influence the healing rate, we screened the following donor characteristics to investigate possible influence corneal healing rate: gender, septic condition (with a donor being considered septic when, before decease, had clinical symptoms or haematochemical evidence of systemic infection), post-mortem time (the time interval between donor's decease and the cornea procurement), death to experiment start time, diabetic condition (diabetic/non-diabetic), stromal defects at procurement (yes/no), heart beating (HB) vs non heart beating (NHB) donor, fevery/non-fevery (fevery defined as a patient with body temperature higher than 37 °C). These parameters are collected from the patient's medical chart by a medical doctor according to the "Guide to the quality and safety of TISSUES AND CELLS for human application (EDQM 5th edition)", Italian National Guidelines and FBOV standard operating system and recorded for each donor through a digital management system. The selection of donor characteristics for the subgroup analysis was performed by a biostatistician (EF) from FBOV.

2.5. Histology analysis

For histological characterization of the damaged tissues, corneal epithelium was removed from five (n = 5) corneas as described above. Three (n = 3) healthy, undamaged tissues were used as a control. Three hours after damage induction, tissues were rinsed 3 times in PBS and fixed with 10 % neutral formaldehyde (Kaltek, Saonara, Italy). Corneas were then cut into four parts, with the first section passing along the diameter of the specimen. The sliced buttons were placed in a metal cassette with pores, that was then taken and emptied into an automatic tissue processor. Tissue embedding was performed in paraffin wax, then cut into 2- to 5-μm thick slices and stained with haematoxylin/eosin (H/E) (Bio-Optica, Milano, Italy) as well as periodic acid-Schiff (PAS, Kaltek, Saonara, Italy). Following preparation, tissues were examined with an optical microscope.

2.6. Bone marrow-derived mesenchymal stromal cells isolation and cultivation

Bone marrow-derived Mesenchymal Stromal Cells (BM-MSCs) were kindly provided by the hematology lab, medicine department of Policlinico G.B. Rossi (Verona), upon obtainment of informed consent, approved by Ethical Committee of Azienda Ospedaliera Universitaria Integrata Verona; (N. 1828, May 12, 2010 "Institution of cell and tissue collection for biomedical research in Onco-Hematology"). Cells were then characterized as previously reported [46–48], as per in Supplementary Fig. 2. BM-MSCs were cultured according to existing literature [24,49] in MEM-α (Ref: 32561–029, Gibco, Life Technologies), supplemented with 10 % Fetal Bovine Serum (Ref: 10099–141, Gibco, Life Technologies), 1 % penicillin-streptomycin (Ref: 11528876, Gibco, Life Technologies) and FGF-β 1 ng/mL (Peprotech, Cat. n. 100-18B) with seeding density of 5000 cells/cm^2.

2.7. Extracellular vesicles isolation and characterization

The MSC-sEV were isolated using size exclusion chromatography (SEC) method from BM-MSCs at passage five. Once cells were at 90 % confluence, the culture medium was removed and cells were rinsed with PBS, followed by starvation for 48 h using Foetal Bovine Serum (FBS)-free medium. The medium was then collected from all the flasks, and underwent a first 300×*g* centrifugation at 4 °C for 10 min and then a second 2000×*g* centrifugation at 4 °C for further 30 min to remove cell debris, smaller debris and apoptotic bodies, respectively. Amicon Ultra-15 centrifugal filter units with 100 kDa molecular weight cut-off (Merck) were then used to concentrate the medium by centrifugation at 3000×*g* for 30 min. The MSC-sEV were isolated from the concentrated medium using qEV-35 nm Original columns (iZON) following manufacturer's instructions. The MSC-sEV were aliquoted in 0.2 μm-filtered PBS and stored at −80 °C until further analysis.

The MSC-sEV then were characterized following MISEV guidelines [22]. The MSC-sEV and QC-100 nm beads as the control were diluted in 0.1 μm filtered water (1:1000) and then were characterized for their size distribution and the concentration by Nanoparticle Tracking Analyser (NTA) using Nanosight NS300 (Malvern zetasizer, Worcestershire, UK).

The morphology of the MSC-sEV was examined by adsorbing 15 μL of the MSC-sEV to Formvar/carbon coated grids, staining by 2 % phosphotungstic acid (PTA) (Ref: HT152, Sigma-Aldrich), air drying, and examining by Hitachi 7500 transmission electron microscope (TEM) at an accelerating voltage of 75 kV.

For immunoblotting, the whole cell and MSC-sEV were lysed in 1x RIPA buffer in order to extract the total protein. The lysates were centrifuged at 4 °C and the protein assay kit (Pierce, Rockford, IL) was used to evaluate the protein concentrations; 40 μg of whole cell lysate and 20 μg of MSC-sEV protein were mixed with 4X NuPage Loading Buffer (Thermofisher) and 2-mercaptoethanol (Sigma-Aldrich, St. Louis, MO, USA), and heated to 95 °C for 5 min using a heat block (Eppendorf). The proteins were resolved on 4–10 % polyacrylamide sodium dodecyl sulphate (Sigma-Aldrich, St. Louis, MO, USA) gels (1 mm thickness), and run in Tris-Glycine (Sigma-Aldrich, St. Louis, MO, USA) running buffer at constant 200 V for 30 min. The resolved proteins were then transferred to polyvinylidene difluoride membranes (Sigma-Aldrich, St. Louis, MO, USA) using a mini-Protean II blotting system (Biorad) at

constant 100 V for 90 min. Afterwards, the membranes were blocked for non-specific binding with 1X Tris-buffered saline (TBS) supplemented with 5 % (w/v) bovine serum albumin (Sigma-Aldrich, St. Louis, MO, USA) for 1 h at room temperature, followed by three washed for 10 min at 4 °C with 1X TBS-T (TBS + 0.1 % Tween-20 (Sigma-Aldrich, St. Louis, MO, USA)). The membranes were incubated overnight at 4 °C with primary antibodies, TSG101 (BioLegend, Cat. No. 934301, 1/500) and Calnexin (BioLegend, Cat. No. 699401, 1/1000) in 5 % BSA-TBS-T buffer. Then, the membranes were washed for 10 min at 4 °C three times with 1X TBS-T. The membranes were incubated for 1 h at room temperature in HRP goat anti-rat IgG (BioLegend, Cat. No. 405405, 1/5000) in 5 % BSA-TBS-T buffer. The blots were washed twice with TBS-T for 10 min and once with TBS for 15 min at room temperature. The membranes were treated with 200 μL of SuperSignal™ West Pico HRP substrate (Thermofisher, USA) in order to develop the chemiluminescence and then were scanned by Image Lab 6.1 software using Biorad Gel Doc system (BioRad, USA) to digitally visualize the protein bands.

The surface marker expression of the MSC-sEV was measured by flow cytometry using Northern Light 3000 (Cytek). 2.5e+8 MSC-sEV were stained by CD9 (Biotechne), CD63 (BD Phamaceutics), and CD81 (BD Phamaceutics) antibodies at concentration of 1:20 in 0.1 μm filtered PBS for 2 h at room temperature protected from light. Forward scatter (FSC) and side scatter (SSC) voltages were set using Apogee size calibration beads, to ensure size ranges from 100 nm to 1300 nm were resolved on the acquisition screen. Besides, 0.1 μm-filtered PBS was run to determine background noise in the buffer and machine.

2.8. Human corneal wound healing model

Human corneal epithelial cells (HCEpi) were a gift from Dr. Araki-Sasaki and colleagues [50]. The HCEpi cells were seeded at a density of 25,000 cells/cm^2 in 12 well-plates. The HCEpi cells were cultured in low glucose (1 g/L) Dulbecco's Modified Eagle Medium (DMEM), supplemented with 0.1 % FBS, and 1 % penicillin/streptomycin. The media were changed every 3 days until full confluence was achieved. Then the media were aspirated and a linear scratch in the middle of the well was applied using a sterile 200 μL pipette tip (Cruinn Diagnostics, Ireland). Afterwards, the cells were rinsed with PBS twice to remove all cell debris. One mL of regular medium as the control or 1 mL of regular medium supplemented with 1×10^8 MSC-sEV/mL as the low dose treatment or 1×10^9 MSC-sEV/mL as the high dose treatment was added into each well. The treatments were added only once after the scratch applied. The cells were then incubated at 37 °C, with 5 % CO_2. Bright field images were taken at 0 h, 18 h, 24 h, and 30 h time points post-scratch using an Olympus CKX53 inverted fluorescent microscope. Wound closure rates at different time points were evaluated according to the wound area calculated by the Olympus CellSens Standard 1.17 software.

2.9. Evaluation of epithelial healing of MSC-sEV treated corneas

Six pairs (n = 12) of human corneoscleral tissues from six (n = 6) donors were used to investigate the influence of MSC-sEV on corneal epithelial healing. Once procured, each tissue pair underwent 1-heptanol epithelial damage as described above. Corneas were rinsed in PBS to remove excess 1-heptanol and then organ-cultured for 3 h in order to allow the complete detachment of the epithelial tissue. For each tissue pair, one tissue was randomly assigned to the untreated (control) group, while the paired cornea was assigned to the treatment group. The control group received the vehicle solution without MSC-sEV, specifically phosphate-buffered saline solution (PBS). The treatment group received a suspension of PBS containing 1.5×10^9 MSC-sEV. On day 0, the day of damage induction, the suspension was applied in a single dose 3 h after damage induction. On days 1, 2, 3, and 4 following damage induction, MSC-sEV administration was divided into three doses of 5×10^8 MSC-sEV, each administered at intervals of 3 h. For the administration, the two suspensions were slowly dropped with a Gilson micropipette on top of the corneal epithelium.

2.10. Statistical analysis

Multiple t-tests were used to analyse the difference in healing rate between FL and TB staining at 24, 48, 72 and 96 h. Correlation followed by linear regression was used to correlate FL and TB staining. Two-tailed unpaired *t*-test was used to measure the difference between subgroups of donors. One-way ANOVA, following Tukey's post hoc test, was applied to measure the difference between treated and control groups of HCEpi. Two-tailed paired *t*-test was employed to determine the statistical difference in every pair of corneas (treated vs non-treated). A p value < 0.05 was considered statistically significant (confidence interval: 95 %). Results are presented as mean ± standard deviation (SD). All data was processed with GraphPad Prism software 8.0 (GraphPad Software, Inc., San Diego, CA, USA).

3. Results

3.1. Human cornea morphology following 1-heptanol damage

Corneoscleral tissues were fixed either healthy (n = 3) or after 1-heptanol damage induction (n = 5) to examine the corneal layers. Histological analysis via H/E staining (Fig. 2) revealed the traditional, five-layered structure of the human cornea (Fig. 2A), with an epithelium made up by 4–5 layers of cells (Fig. 2B). The 1-heptanol-damaged corneas were instead denuded from the epithelium (Fig. 2C), and the stroma was no to mildly oedematous. Interestingly, although the corneal epithelium was detached, Bowman's layer remained morphologically unaltered in both structure and thickness and a normal epithelial morphology was observed in the periphery not subjected to 1-heptanol damage (Fig. 2D). No significant alterations were observed in the Descemet membrane or in the endothelium (Fig. 2C).

3.2. Corneal epithelial healing kinetics

The healing kinetics of corneoscleral tissues following chemical damage were studied in 68 tissues. The repeatability of the quantification damaged epithelial area by manual drawing of the ROI on acquired images, expressed as CV%, was 1.02 % and 1.15 % for, respectively, FL and TB staining techniques. Supplementary Fig. 3 shows Bland-Altmann plots for determination of bias on HR values introduced by interoperator variability, both in FL (Supplementary Fig. 3A) and TB (Supplementary Fig. 3B) staining techniques. Bland-Altman plot gave a non-significant bias between operators both for FL (average bias: 0.26 mm^2; 95 % confidence intervals: [−0.32; 0.85]; *p*: 0.4) and for TB (average bias: 0.36 mm^2; 95 % confidence intervals: [−0.34; 1.07]; *p*: 0.3) analysis. Fig. 3A shows a representative recovery pattern of a damaged tissue, both for after FL staining (upper panel) as well as for TB staining (lower panel), demonstrating considerable healing activity within the first 48 h. Fig. 3B depicts a graph with healing rates, with both the healing rates HR^{FL} and HR^{TB} peaking at 48 h after damage. Notably, TB staining indicates a higher HR compared to FL staining at 24 h ($p = 0.0452$, effect size = 0.3468), 48 h ($p = 0.0025$, effect size = 0.5291), and 72 h ($p = 0.0498$, effect size = 0.3394), whereas at 96 h, the healing rate levels off to similar values for both staining techniques. In terms of damaged area, TB staining initially marks a larger area than FL staining ($p = 0.0013$, effect size = 0.5648) on day 0, as soon the damage is exerted (Fig. 3C). While no differences are observed at 24 and 48 h, at 72 and 96 h FL staining reveals a larger damaged area compared to TB staining ($p = 0.0143$, effect size = −0.4255; $p = 0.0165$, effect size = −0.4163). Despite providing different insights due to their distinct structures, the two staining techniques showed a positive correlation ($R^2 = 0.3170$; $p < 0.0001$), indicating coherent information regarding the healing process

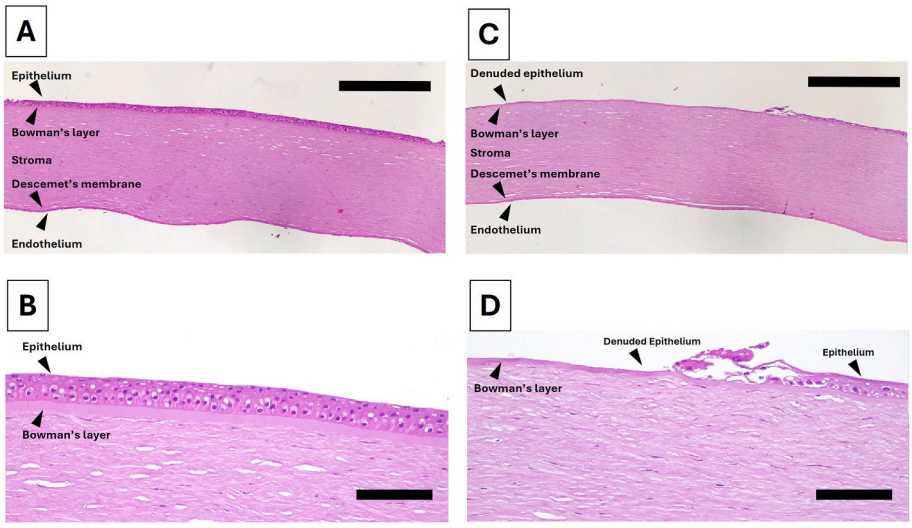

Fig. 2. representative images of histological analysis after H/E staining on healthy and 1-heptanol damaged corneas in the central epithelial area. (A) Bright field image of the healthy cornea at 5x magnification with constituent layers labelled. (B) Bright field image showing a detailed magnification at 20x from (A). (C) Bright field image of the 1-heptanol damaged cornea at 5x magnification with constitutent layers labelled. (D) Bright field image showing a detailed magnification at 20x from (C).

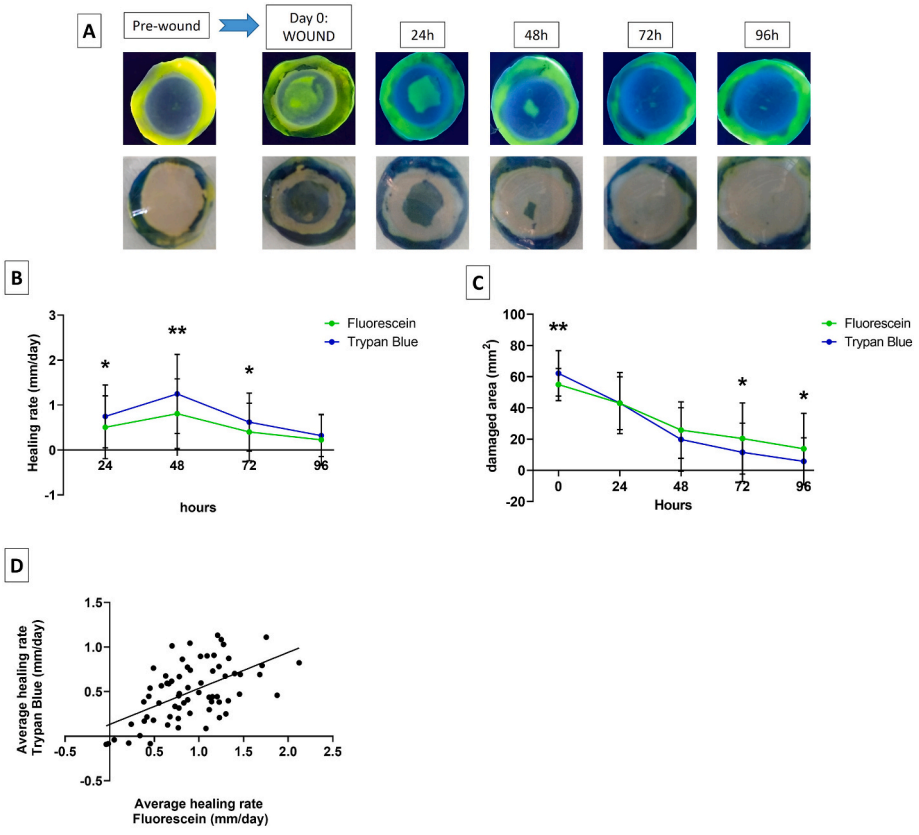

Fig. 3. human corneal 1-heptanol wounding and repair kinetics monitored with fluorescein (FL) and trypan blue (TB) staining. (A) Kinetics images of a representative cornea, whose epithelium was wounded with 1-heptanol (Day 0 Post-wound), followed by healing in corneal culture at 31 °C up to 96 h of organ culture, assessed by FL (upper panel) and TB (lower panel) staining. The absence of epithelial damage and alteration prior to chemical damage (Day 0 Pre-wound) was also evaluated. (B) Graph illustrating the average ± standard deviation HR of corneas at each evaluated time point, measured with FL (HR^{FL}, green line) and TB (HR^{TB}, blue line) staining. (C) Graph depicting the average ± standard deviation size of the damaged area over time, measured with FL (green line) and TB (blue line) staining. (D) Correlation between the average healing rate (HR_{avg}) measured with TB (y-axis) and HR_{avg} measured with FL (x-axis). Graphs include data from a sample size of n = 68 corneas. *: $p < 0.05$; **: $p < 0.01$. (For interpretation of the references to colour in this figure legend, the reader is referred to the Web version of this article.)

(Fig. 3D).

3.3. Effect of donor characteristics on corneal epithelial repair

Although the majority of tissues exhibited a consistent recovery trend, some showed reduced healing capacity. To investigate this further, we examined the influence of donor characteristics on the healing potential of 1-heptanol damaged corneal epithelia.

Donor parameters such as gender, sepsis, fever, diabetes, post-mortem time, procurement to experiment start time, stromal defects at procurement did not show significant differences (Supplementary Tables 1 and 2; Supplementary Fig. 4). However, two factors emerged that negatively impacted the healing process in specific patient subgroups. Fig. 4A and B and Supplementary Fig. 5A show the HR_{avg} measured with FL and TB staining, respectively, in non-diabetic and diabetic donors. The recovery process was significantly slower in the diabetic subgroup, as measured by both staining techniques ($p = 0.0340$, effect size $= -0.6914$ FL; $p = 0.0382$, effect size $= -0.7195$ TB), compared to non-diabetic donors.

Fig. 4C and D and Supplementary Fig. 5B present the HR_{avg} measured with FL and TB staining, respectively, in non-heart-beating (NHB) versus heart-beating (HB) brain-deceased donors. FL staining revealed a slower healing rate in HB donors compared to NHB donors ($p = 0.0499$, effect size4 $= -0.6293$), whereas TB staining did not show a statistically significant difference ($p = 0.1556$, effect size $= -0.4475$).

3.4. MSC-sEV characterization

Small extracellular vesicles (sEV) were isolated from MSC conditioned medium with SEC. Characterization of MSC-sEV size distribution and concentration was analysed by NTA, and revealed a mode size of 79.8 nm and a concentration of 2.5 x 10^10 particles/mL (Fig. 5A), which was validated by analysing QC-100 nm beads (Malvern) (Supplementary Fig. 6). TEM was employed to examine the morphology of the MSC-sEV, illustrating bilayer particles within the desired size range of 80 nm and spherical shape (Fig. 5B).

Western blot analysis was performed to characterize the MSC-sEV for TSG101 as a cytosolic marker and Calnexin as a negative marker. The cytosolic protein TSG101 (45 KDa) was detected and shown to be positive for MSC-sEV samples. Calnexin (90 KDa) was negative for MSC-sEV group, but it was observed in the blot from whole cell sample (Fig. 5C).

Flow cytometry was conducted to characterize the surface biomarkers of the MSC-sEV. The gating strategy, side scatter and forward scatter voltage adjustment using Apogee beads (Apogee flow systems, UK), and dot plot analysis are shown in Supplementary Fig. 7. The surface biomarker expression of the MSC-sEV compared to the unstained MSC-sEV as the control group was 67.8 %, 83.8 %, and 77.3 % positive for CD9, CD63, and CD81, respectively.

3.5. MSC-sEV promote wound healing in vitro

To evaluate the effect of MSC-sEV on epithelial healing, a wound healing assay was conducted on human corneal epithelial cells (HCEpi). No significant differences were observed between the control group and the low dose (1×10^8 MSC-sEV/mL) and high dose (1×10^9 MSC-sEV/mL) MSC-sEV groups at 18- and 24-h post-scratch induction (Supplementary Fig. 8). However, at 30 h post-scratch, the wounded area of the HCEpi receiving low dose MSC-sEV treatment was reduced to 12 % ± 9 % of the original wound size. The HCEpi administered with high dose MSC-sEV showed a reduction to 3 % ± 3 % of the original wound size at 30 h post-scratch time, while the control group only healed up to 27 % ± 11 % of the initial wound size (Fig. 6A and C). A significant improvement in cell migration and reepithelialisation was observed in the group receiving the high dose of EVs compared to the control group ($p = 0.0438$) at 30 h post-scratch time point (Fig. 6B).

3.6. MSC-sEV administration enhance epithelial healing on human corneas

To investigate whether the positive effect in wound healing observed with MSC-sEV administration *in vitro* could be replicated in an *ex vivo* model, we conducted experiments exploiting the established damage model on human corneoscleral tissues. Twelve human corneas from six donors were divided into two groups, with one cornea assigned to the

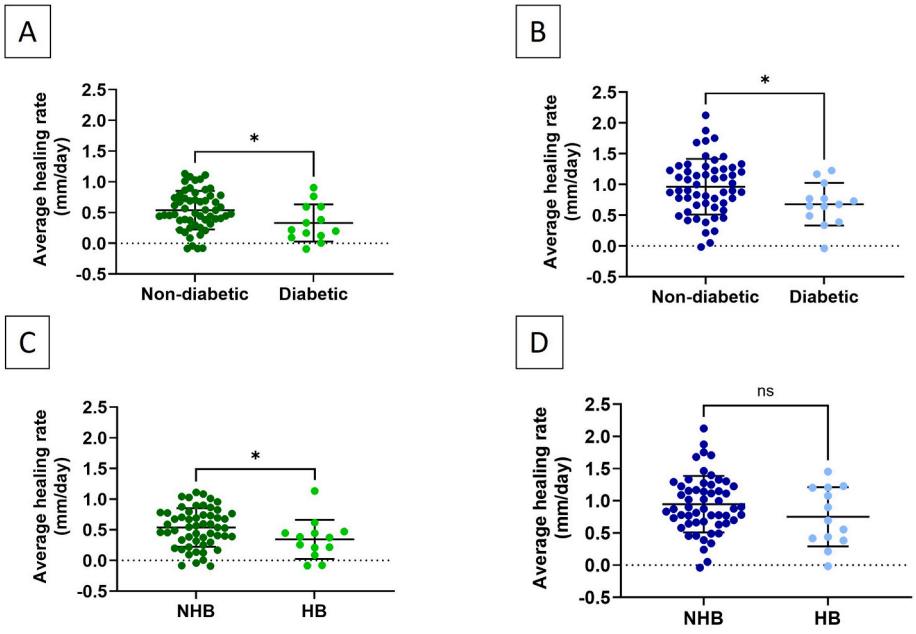

Fig. 4. Influence of donor cornea characteristics on epithelial repair after 1-heptanol damage. (A) and (B): scatter plots showing average ± standard deviation of average healing rate (HR_{avg}) of corneas from non-diabetic (n = 13) and diabetic (n = 55) donors, obtained after FL (A) and TB (B) staining. (C) and (D): graphs showing average ± standard deviation of HR_{avg} of corneas from Non-Heart Beating (NHB, n = 13) and Heart Beating (HB, n = 55) donors, obtained from FL (C) and TB (D) measurements. *: $p < 0.05$.

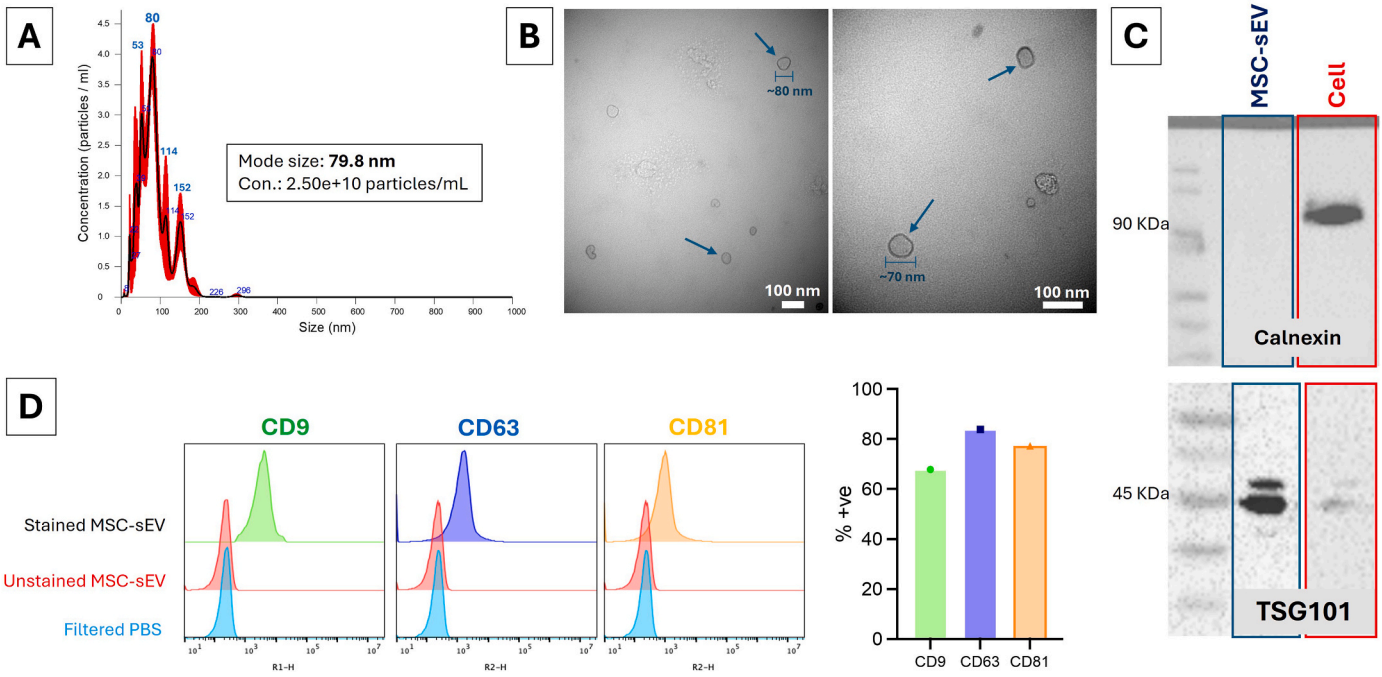

Fig. 5. MSC-sEV characterization. (A) NTA analysis showing the size distribution of the MSC-sEV and their concentration. (B) TEM imaging with 120,000x and 200,000x direct magnifications illustrating the spherical morphology of the MSC-sEV and their size. (C) Western blot analysis illustrating the presence of the TSG101 as a positive cytosolic marker and Calnexin as a negative marker in MSC-sEV group, and the Calnexin presence in whole cell lysate. (D) Flow cytometry analysis of the MSC-sEV tetraspanin markers showing the expression of the CD9, CD63, and CD81 on the surface of the MSC-sEV compared to the unstained group.

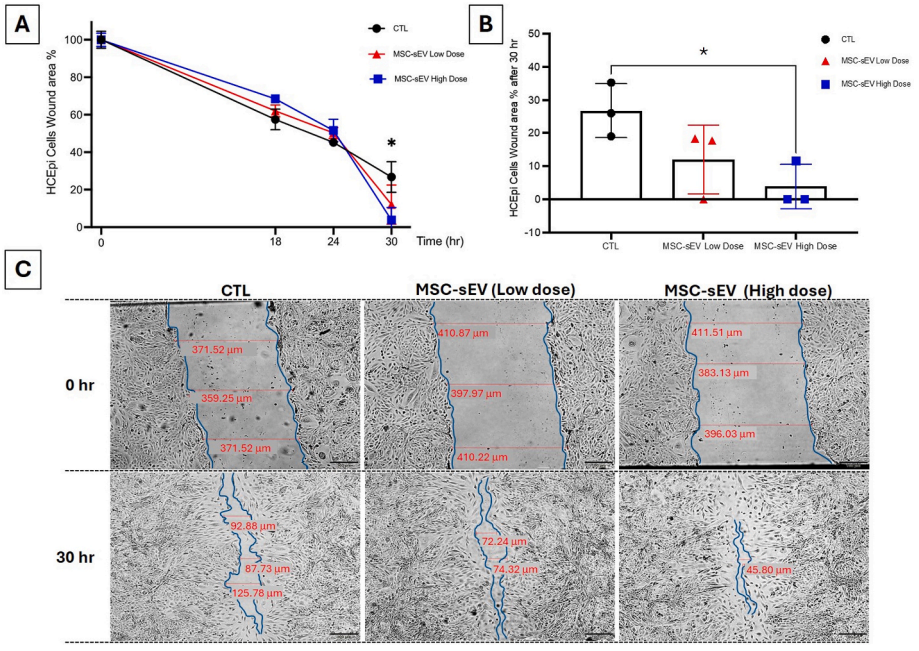

Fig. 6. MSC-sEV effect on HCEpi cells scratch model. (A) measurement of wounded area healing for each group at 0, 18, 24 and 30 h post scratch. (B) Wound area measurement at 30 h post-scratch for MSC-sEV treated and control groups. (C) Wound images for each group of treatment: control, low dose, and high dose of MSC-sEV at 0 and 30 h post scratch. *: $p < 0.05$.

control group and the other to the treatment group, thus mitigating donor-related variability. As shown in Fig. 7A, tissues treated with MSC-sEV exhibited a significantly higher HR_{avg} compared to the untreated controls ($p = 0.004$, effect size = 1.097). Fig. 7B depicts representative images of the healing processes in both groups, monitored with FL staining.

Interestingly, this intergroup difference was not observed with TB staining. Specifically, Fig. 7C shows the healing rate between treated and untreated tissues, monitored with TB, with no significant differences highlighted among the two groups ($p = 0.2071$, effect size = 0.2755). This can be explained by the fact that MSC-sEV can stimulate tissue repair but not reverse cell death. Fig. 7D presents representative images of the healing process in both groups as visualized by TB staining.

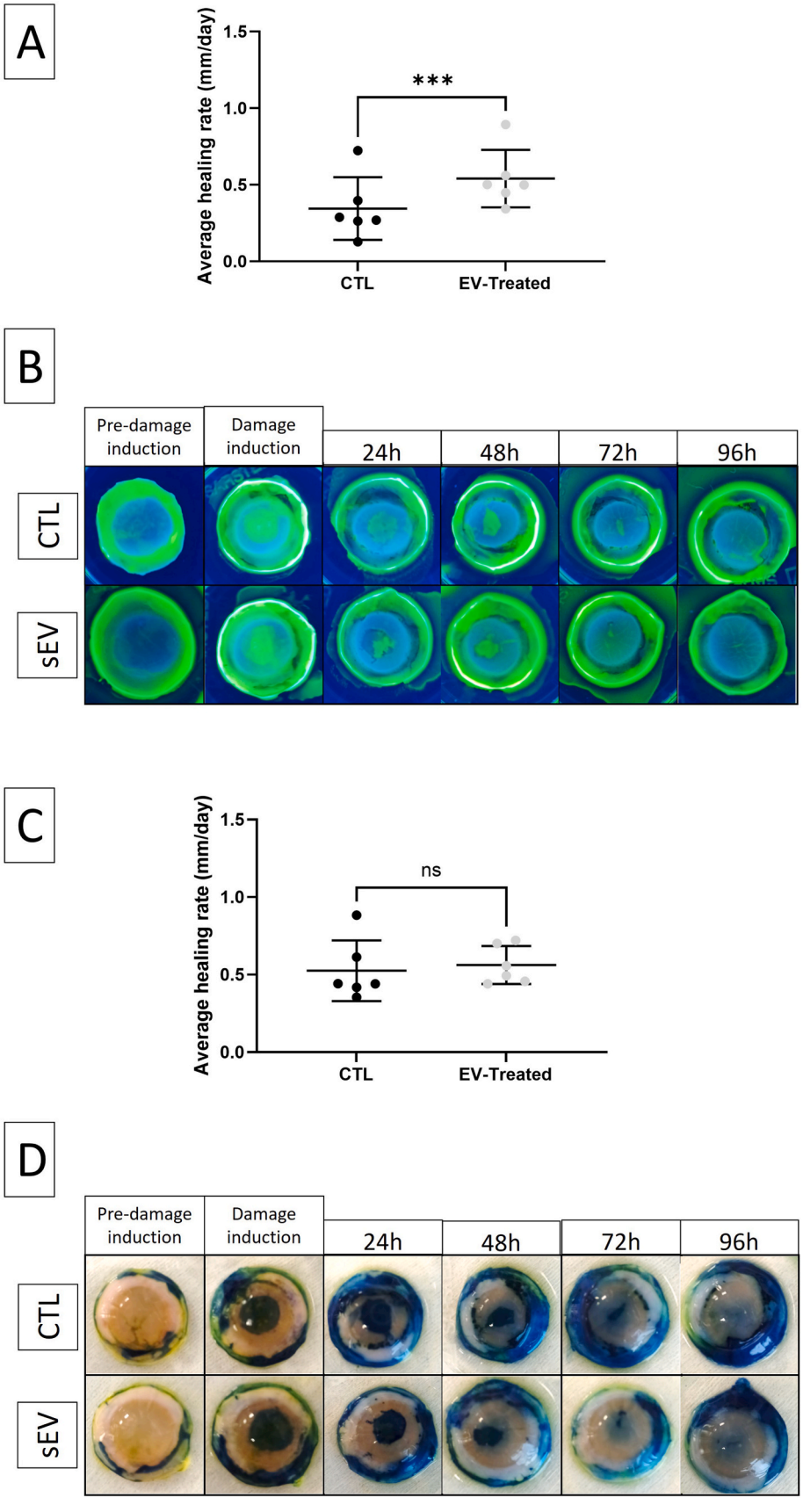

(caption on next page)

Fig. 7. Effect of MSC-sEV administration on tissues with chemically-induced epithelial damage. (A) Scatter plot depicting the average healing rate ± standard deviation, as measured by FL staining, in untreated (n = 6) versus treated (n = 6) corneoscleral tissues. (B) Representative images of the healing process in control and treated corneoscleral tissues at the time of damage induction and at 24, 48, 72, and 96 h post-damage induction as revealed by FL staining. (C) Scatter plot depicting the average healing rate ± standard deviation, as measured by TB staining, in untreated (n = 6) versus treated (n = 6) corneoscleral tissues. (D) Representative images of the healing process in control and treated corneoscleral tissues at the time of damage induction and at 24, 48, 72, and 96 h post-damage induction as revealed by TB staining. ***: $p < 0.001$.

4. Discussion

In the present study, we established an innovative model for studying ex *vivo* corneal epithelial repair using selective chemical damage with 1-heptanol. During the characterization of the model, we found that epithelial repair is achieved within 96 h in corneal organ culture at 31 °C and that the process is significantly slower in corneas from diabetic and heart-beating donors. We then investigated the healing potential of human bone marrow MSC-sEV, first in an *in vitro* setting on human corneal epithelial cells and subsequently *ex vivo* on the established model, proving its applicability for testing corneal epithelial repair.

Our work showed that corneal epithelial damage induced by a paper disc soaked in 1-heptanol precisely affects a circumscribed area, inducing cell death via necrosis. Indeed, the acute and overwhelming cytotoxic effects of pure 1-heptanol causes immediate and catastrophic damage to cellular structures, dissolving the lipid bilayer of cell membranes and leading to loss of integrity and uncontrolled leakage of cellular contents. Moreover, this approach does not compromise the integrity of Bowman's layer, nor that of the other corneal layers. This is particularly important because other methods described in the literature, such as scraping and alkali burns, may cause damage to the underlying corneal layers [2]. Although the function of Bowman's layer is not yet fully understood, the most widely accepted hypothesis suggests its primary role is to mediate chemotactic communication between corneal epithelial cells and underlying keratocytes [51]. Therefore, for corneal epithelial repair studies, it is preferable to use a damage model that does not disrupt Bowman's layer. Another advantage of the presented model is the reproducibility of the damage. Due to the hydrophobic properties of 1-heptanol and the use of a standard-sized paper disc it is possible to induce localized damage avoiding operator-dependent variability.

The use of 1-heptanol for studying corneal epithelial repair in human corneas *ex vivo* was previously described by Ljubimov and collaborators [14–16] showing that corneas from donors with diabetic retinopathy have impaired epithelial healing capacity. This adverse effect was found to be associated with dysfunctional diabetic pathways and alterations of adhesive molecules in the epithelial basement membrane [14–16]. However, in their studies, the healing rate was monitored through phase-contrast imaging and operator-dependent judgment. In our study, we provide, for the first time, a comprehensive characterization and kinetics of the healing rate of human corneoscleral tissues measured through the two vital dyes FL and TB. To make the analysis more objective and standardized, we adapted a previously reported analysis system to measure the wounded area [45]. Through this system, we converted the wounded area from pixels into mm^2, obtaining a healing rate coefficient representative of the speed of wound closure. Our findings demonstrate that healing activity peaks around 48 h following damage induction and progresses towards full recovery after 96 h. Although showing a similar trend, TB staining revealed a higher healing rate in the first 72 h and a smaller damaged area at both 72 and 96 h compared to FL staining. We hypothesize that this is due to the different tissue penetration mechanisms of the two dyes. Indeed, the relatively high molecular weight TB (molecular formula $C_{34}H_{24}N_6Na_4O_{14}S_4$; 873 Da) is exclusively internalized by injured or dead epithelial cells with a damaged plasma membrane [40,41], while the lower molecular weight FL (molecular formula $C_{20}H_{10}Na_2O_5$; 376 Da) can permeate via paracellular entry through adjacent cells due to the lack of superficial glycocalyx and of fully functional tight junctions in a not completely healed epithelium [39]. Accordingly, significant differences in wounded areas detected by TB and FL staining were highlighted. This is consistent with the faster healing rate observed with TB than with FL, suggesting that the covering of denuded Bowman layer by epithelial cells precedes the complete establishment of epithelial barrier integrity, resulting in TB-negative and FL-positive zones. Noteworthy, while providing different information, both FL and TB staining were consistent in tracking the process of corneal epithelial repair.

Following the initial characterization of the healing process, we examined whether certain donor subpopulations exhibit different recovery profiles. Screening multiple characteristics, we found that recovery is slower in diabetic donors, consistent with previous literature [14–16,52–55]. Key contributing factors include the disruption of growth factor signalling [56,57], increased oxidative stress [57], altered protease activity [58], accumulation of advanced glycation end-products in the epithelium-basement membrane complex [57], impaired corneal innervation [59], and dysregulation of the immune response [60]. Additionally, we report for the first time that heart-beating (HB) brain-deceased donors also show a slower healing rate compared to non-heart-beating donors, as revealed by FL staining. Although we do not provide direct evidence, we speculate that the death of the HB donor's central nervous system may negatively influence nervous tissue homeostasis, given that the cornea is the most innervated organ in the human body [61]. In addition, physiological instability [62,63], increased inflammatory response [64,65] and organ's microenvironment alteration, disturbed cardiovascular activity [66], hormonal imbalances [67,68], metabolic alterations [67], coagulation abnormalities [67] and imbalanced body temperature [67] can lead to a significant loss of quality in procured tissues for transplant [69]. Our findings highlight the crucial importance of selecting the appropriate tissue for *ex vivo* research. We demonstrated that certain donor parameters significantly influence the outcome of epithelial recovery, potentially leading to biased results. Therefore, it is essential to consider the donor's medical history when investigating corneal epithelial healing.

After fully characterizing our damage model, we aimed to demonstrate its usefulness for studying corneal epithelial repair. MSC-EVs have emerged over recent decades as powerful tools in regenerative medicine, playing active roles in tissue repair and modulating inflammation and immune response [23–26]. Their therapeutic activity is mediated by the release of their cargo, which includes proteins, mRNAs, miRNAs, DNA, lipids, growth factors and mitochondria upon fusion and intake by the recipient cell [46,47]. Recent applications in ophthalmology have shown that MSC-EVs accelerate wound healing in *in-vitro* and *in-vivo* corneal scratch models [32], in a cornea-on-a-chip model [70] and in murine models of corneal alkali burn [71,72].

In this work, we show that our MSC-sEV have a mode size of 79 nm, classifying them as small extracellular vesicles according to the latest MISEV guidelines [22]. We first tested MSC-sEV administration on *in vitro* cultured human corneal epithelial cells, showing that a low dose (1×10^8 particles/mL) had no significant effect, while a high dose (1×10^9 particles/mL) significantly enhanced wound closure at 30 h. This result obtained in a bidimensional model led us to further investigate the effect of the MSC-sEV administration on our established *ex vivo* model, in order to measure their effect on a more complex system closely mimicking an *in vivo* one. Our results show that MSC-sEV-treated corneas have a significantly higher healing rate as measured by FL staining but not by TB. This finding was expected, as MSC-sEV can enhance tissue repair, but not reverse cell death.

Our results support future new opportunities in the management of corneal epithelial diseases using MSC-sEV. Currently, corneal ulcers, neurotrophic ulcers, abrasions, and other diseases that disrupt the epithelial barrier (i.e. dry eye disease) are managed through the administration of eye drops containing different kinds of biologically active substances. These include amniotic membrane extract eye drops [73], serum eye drops [74], insulin eye drops [74,75] and Nerve Growth Factor (NGF) eye drops [76,77]. The use of extracellular vesicles for the management of ocular surface diseases has many advantages. First, Good Manufacturing Practice (GMP) manufacturing strategies for the production of BM-MSC-EVs for phase I and II clinical studies have already been established [20,78–80]. Therefore, a substantial body of literature witnesses the safety and biocompatibility of MSC-EVs. Additionally, the role of MSC-EVs in regenerative medicine is under investigation in multiple clinical trials. To the best of our knowledge, no clinical trials assessing the effect of MSC-sEV in corneal epithelial repair have been conducted to date. However, in a similar context, clinical trials are investigating the safety of topical MSC-EVs-based ointments on healthy subjects (ID: NCT05523011) and the role of MSC-EVs in epithelial wound healing in individuals affected by Dystrophic Epidermolysis Bullosa (ID: NCT04173650). The existing evidence in literature and medical practice regarding the benefits of MSC-EVs administration strengthens their potential use in ophthalmology.

This study has a number of limitations that warrant discussion. Firstly, although the use of paired corneoscleral tissues from the same donor allowed for direct comparison between MSC-sEV-treated samples and their corresponding controls, the overall sample size was limited. This small sample size may impact the statistical power of our findings. Future studies with a larger cohort and careful titration of MSC-sEV dosages are necessary to validate and expand upon our results. Secondly, the repeated administration of the MSC-sEV solution three times daily may have contributed to a cumulative effect, which could influence the observed outcomes. Further investigations should explore different dosing regimens to clarify this aspect. Also, a more thorough dose/response study would allow to optimize the working concentration. Finally, while our *ex vivo* model offers several advantages—including adherence to the 3R principles, close resemblance to the *in vivo* environment, and the use of human tissues—it remains an *ex vivo* system. As such, it cannot fully replicate the complex dynamics of an *in vivo* setting, which may limit the generalizability of our findings.

In conclusion, our work provides a novel, animal-free *ex vivo* model for studying corneal epithelial repair. We characterized the recovery kinetics in the 96 h following damage induction using FL and TB to monitor barrier function and epithelial viability. We identified donor parameters influencing recovery speed and demonstrated the healing potential of the human bone marrow mesenchymal stromal cells derived extracellular vesicles in our *ex vivo* model, opening up perspectives for their use in managing corneal epithelial pathologies.

CRediT authorship contribution statement

Filippo Bonelli: Writing – review & editing, Writing – original draft, Project administration, Methodology, Investigation, Formal analysis, Data curation, Conceptualization. **Seyedmohammad Moosavizadeh:** Investigation, Data curation. **Elisa Fasolo:** Investigation, Formal analysis. **Alessia Di Nella:** Investigation. **Vanessa Barbaro:** Writing – review & editing. **Ilaria Zorzi:** Formal analysis. **Mauro Krampera:** Writing – review & editing. **Jana D'Amato Tóthová:** Writing – review & editing. **Diego Ponzin:** Funding acquisition. **Thomas Ritter:** Writing – review & editing, Funding acquisition. **Stefano Ferrari:** Writing – review & editing, Supervision, Funding acquisition. **Umberto Rodella:** Writing – review & editing, Writing – original draft, Project administration, Methodology, Investigation, Formal analysis, Data curation, Conceptualization.

Declaration of generative AI and AI-assisted technologies in the writing process

During the preparation of this work the authors used ChatGPT (OpenAI) in order to improve language and readability. After using this tool/service, the authors reviewed and edited the content as needed and take full responsibility for the content of the publication.

Funding sources

This work was partially supported by "5x1000" funds for scientific research from the Italian Ministry of Health and the Italian Ministry of University & Research, by the Science Foundation Ireland 18/EPSRC-CDT/3583, by the Engineering and Physical Sciences Research Council EP/S02347X/1, by a grant from Science Foundation Ireland (SFI) and the European Regional Development Fund (ERDF) under grant number 13/RC/2073_P2 (S.M. and T.R.) and by a Short-Term Scientific Mission grant to FB from the European Cooperation in Science and Technology (EU-COST) Action CA18116 "Aniridia: networking to address an unmet medical, scientific, and societal challenge".

Conflicts of interest

None to declare.

Acknowledgements

The authors would like to thank Moreno Piaia (Fondazione Banca degli Occhi del Veneto ETS) and Anastasia Walsh (Discipline of Pharmacology and Therapeutics, School of Medicine, Nursing and Health Sciences, University of Galway) for kind experimental support during the revision phase.

Appendix A. Supplementary data

Supplementary data to this article can be found online at https://doi.org/10.1016/j.jtos.2025.02.002.

References

[1] DelMonte DW, Kim T. Anatomy and physiology of the cornea. J Cataract Refract Surg 2011;37:588–98. https://doi.org/10.1016/j.jcrs.2010.12.037.
[2] Zhao J, Nagasaki T. Mechanical damage to corneal stromal cells by epithelial scraping. Cornea 2004;23:497–502. https://doi.org/10.1097/01.ico.0000114129.63670.ab.
[3] Hung KH, Yeh LK. Ex vivo and in vivo animal models for mechanical and chemical injuries of corneal epithelium. J Vis Exp 2022. https://doi.org/10.3791/63217.
[4] Villabona-Martinez V, Sampaio LP, Shiju TM, Wilson SE. Standardization of corneal alkali burn methodology in rabbits. Exp Eye Res 2023;230:109443. https://doi.org/10.1016/j.exer.2023.109443.
[5] Luisi J, Lin JL, Karediya N, Kraft ER, Sharifi A, Schmitz-Brown ME, et al. Concentration-associated pathology of alkali burn in a mouse model using anterior segment optical coherence tomography with angiography. Exp Eye Res 2022;223:109210. https://doi.org/10.1016/j.exer.2022.109210.
[6] Heinonen T. Better science with human cell-based organ and tissue models. Altern Lab Anim 2015;43:29–38. https://doi.org/10.1177/026119291504300107.
[7] Cintron C, Hassinger L, Kublin CL, Friend J. A simple method for the removal of rabbit corneal epithelium utilizing n-heptanol. Ophthalmic Res 1979;11:90–6. https://doi.org/10.1159/000264990.
[8] Sakai O, Uchida T, Imai H, Ueta T. Glutathione peroxidase 4 plays an important role in oxidative homeostasis and wound repair in corneal epithelial cells. FEBS Open Bio 2016;6:1238–47. https://doi.org/10.1002/2211-5463.12141.
[9] Fukuda M, Sasaki H. Quantitative evaluation of corneal epithelial injury caused by n-heptanol using a corneal resistance measuring device in vivo. Clin Ophthalmol 2012;6:585–93. https://doi.org/10.2147/OPTH.S30935.
[10] Fukuda M, Sasaki H. Effects of fluoroquinolone-based antibacterial ophthalmic solutions on corneal wound healing. J Ocul Pharmacol Therapeut 2015;31:536–40. https://doi.org/10.1089/jop.2014.0118.
[11] Kimura K, Hattori A, Usui Y, Kitazawa K, Naganuma M, Kawamoto K, et al. Stimulation of corneal epithelial migration by a synthetic peptide (PHSRN) corresponding to the second cell-binding site of fibronectin. Investig Ophthalmol Vis Sci 2007;48:1110–8. https://doi.org/10.1167/iovs.06-0704.

[12] Chung JH, Kim WK, Lee JS, Pae YS, Kim HJ. Effect of topical Na-hyaluronan on hemidesmosome formation in n-heptanol-induced corneal injury. Ophthalmic Res 1998;30:96–100. https://doi.org/10.1159/000055460.
[13] Massie I, Levis HJ, Daniels JT. Response of human limbal epithelial cells to wounding on 3D RAFT tissue equivalents: effect of airlifting and human limbal fibroblasts. Exp Eye Res 2014;127:196–205. https://doi.org/10.1016/j.exer.2014.07.024.
[14] Kabosova A, Kramerov A, Aoki A, Murphy G, Zieske J, Ljubimov AV. Human diabetic corneas preserve wound healing, basement membrane, integrin and MMP-10 differences from normal corneas in organ culture. Exp Eye Res 2003;73:543–62.
[15] Saghizadeh M, Kramerov AA, Yu F shin X, Castro MG, Ljubimov AV. Normalization of wound healing and diabetic markers in organ cultured human diabetic corneas by adenoviral delivery of c-met gene. Investig Ophthalmol Vis Sci 2010;51:1970–80. https://doi.org/10.1167/iovs.09-4569.
[16] Saghizadeh M, Epifantseva I, Hemmati DM, Ghiam CA, Brunken WJ, Ljubimov AV. Enhanced wound healing, kinase and stem cell marker expression in diabetic organ-cultured human corneas upon MMP-10 and cathepsin F gene silencing. Investig Ophthalmol Vis Sci 2013;54:8172–80. https://doi.org/10.1167/iovs.13-13233.
[17] Singh P, Tyagi M, Kumar Y, Gupta KK, Sharma PD. Ocular chemical injuries and their management. Oman J Ophthalmol 2013;6:83–6. https://doi.org/10.4103/0974-620X.116624.
[18] Sharma N, Kaur M, Agarwal T, Sangwan VS, Vajpayee RB. Treatment of acute ocular chemical burns. Surv Ophthalmol 2018;63:214–35. https://doi.org/10.1016/j.survophthal.2017.09.005.
[19] Liang X, Ding Y, Zhang Y, Tse H-F, Lian Q. Paracrine mechanisms of mesenchymal stem cell-based therapy: current status and perspectives. Cell Transplant 2014;23:1045–59. https://doi.org/10.3727/096368913X667709.
[20] Kou M, Huang L, Yang J, Chiang Z, Chen S, Liu J, et al. Mesenchymal stem cell-derived extracellular vesicles for immunomodulation and regeneration: a next generation therapeutic tool? Cell Death Dis 2022;13:580. https://doi.org/10.1038/s41419-022-05034-x.
[21] Pittenger MF, Discher DE, Péault BM, Phinney DG, Hare JM, Caplan AI. Mesenchymal stem cell perspective: cell biology to clinical progress. NPJ Regen Med 2019;4:22. https://doi.org/10.1038/s41536-019-0083-6.
[22] Welsh JA, Goberdhan DCI, O'Driscoll L, Buzas EI, Blenkiron C, Bussolati B, et al. Minimal information for studies of extracellular vesicles (MISEV2023): from basic to advanced approaches. J Extracell Vesicles 2024;13:e12404. https://doi.org/10.1002/jev2.12404.
[23] Merimi M, El-Majzoub R, Lagneaux L, Moussa Agha D, Bouhtit F, Meuleman N, et al. The therapeutic potential of mesenchymal stromal cells for regenerative medicine: current knowledge and future understandings. Front Cell Dev Biol 2021;9:661532. https://doi.org/10.3389/fcell.2021.661532.
[24] Wang J, Donohoe E, Canning A, Moosavizadeh S, Buckley F, Brennan MÁ, et al. Immunomodulatory function of licensed human bone marrow mesenchymal stromal cell-derived apoptotic bodies. Int Immunopharmacol 2023;125:111096. https://doi.org/10.1016/j.intimp.2023.111096.
[25] Seo Y, Kim H-S, Hong I-S. Stem cell-derived extracellular vesicles as immunomodulatory therapeutics. Stem Cell Int 2019;2019:5126156. https://doi.org/10.1155/2019/5126156.
[26] Lynch K, Treacy O, Chen X, Murphy N, Lohan P, Islam MN, et al. TGF-β1-Licensed murine MSCs show superior therapeutic efficacy in modulating corneal allograft immune rejection in vivo. Mol Ther 2020;28:2023–43. https://doi.org/10.1016/j.ymthe.2020.05.023.
[27] Oh JY, Lee RH. Mesenchymal stromal cells for the treatment of ocular autoimmune diseases. Prog Retin Eye Res 2021;85:100967. https://doi.org/10.1016/j.preteyeres.2021.100967.
[28] Jafarinia M, Alsahebfosoul F, Salehi H, Eskandari N, Ganjalikhani-Hakemi M. Mesenchymal stem cell-derived extracellular vesicles: a novel cell-free therapy. Immunol Investig 2020;49:758–80. https://doi.org/10.1080/08820139.2020.1712416.
[29] Nuzzi A, Pozzo Giuffrida F, Luccarelli S, Nucci P. Corneal epithelial regeneration: old and new perspectives. Int J Mol Sci 2022;23:1–16. https://doi.org/10.3390/ijms232113114.
[30] Cabral J, Ryan AE, Griffin MD, Ritter T. Extracellular vesicles as modulators of wound healing. Adv Drug Deliv Rev 2018;129:394–406. https://doi.org/10.1016/j.addr.2018.01.018.
[31] Yu B, Li X-R, Zhang X-M. Mesenchymal stem cell-derived extracellular vesicles as a new therapeutic strategy for ocular diseases. World J Stem Cell 2020;12:178–87. https://doi.org/10.4252/wjsc.v12.i3.178.
[32] Samaeekia R, Rabiee B, Putra I, Shen X, Park YJ, Hematti P, et al. Effect of human corneal mesenchymal stromal cell-derived exosomes on corneal epithelial wound healing. Investig Ophthalmol Vis Sci 2018;59:5194–200. https://doi.org/10.1167/iovs.18-24803.
[33] Yáñez-Mó M, Siljander PR-M, Andreu Z, Zavec AB, Borràs FE, Buzas EI, et al. Biological properties of extracellular vesicles and their physiological functions. J Extracell Vesicles 2015;4:27066. https://doi.org/10.3402/jev.v4.27066.
[34] Silva AM, Teixeira JH, Almeida MI, Gonçalves RM, Barbosa MA, Santos SG. Extracellular Vesicles: immunomodulatory messengers in the context of tissue repair/regeneration. Eur J Pharmaceut Sci 2017;98:86–95. https://doi.org/10.1016/j.ejps.2016.09.017.
[35] Kwok ZH, Wang C, Jin Y. Extracellular vesicle transportation and uptake by recipient cells: a critical process to regulate human diseases. Processes 2021;9. https://doi.org/10.3390/pr9020273.
[36] Balasopoulou A, Kokkinos P, Pagoulatos D, Plotas P, Makri OE, Georgakopoulos CD, et al. Factors affecting the epithelial integrity of human donor corneas Amanjot. Indian J Ophthalmol 2022. https://doi.org/10.4103/ijo.IJO.
[37] Kim T, Palay DA, Lynn M. Donor factors associated with epithelial defects after penetrating keratoplasty. Cornea 1996;15:451–6.
[38] Van Meter WS, Katz DG, White H, Gayheart R, Sugar A, Linsy Farris R, et al. Effect of death-to-preservation time on donor corneal epithelium. Trans Am Ophthalmol Soc 2005;103:209–24.
[39] Bron AJ, Argüeso P, Irkec M, Bright FV. Clinical staining of the ocular surface: mechanisms and interpretations. Prog Retin Eye Res 2015;44:36–61. https://doi.org/10.1016/j.preteyeres.2014.10.001.
[40] Riss T, Niles A, Moravec R, Karassina N, Vidugiriene J. Cytotoxicity assays: in vitro methods to measure dead cells. In: Markossian S, Grossman A, Arkin M, Auld D, Austin C, Baell J, et al., editors. AAssay guidance manual [internet]. Bethesda (MD): Eli Lilly & Company and the National Center for Advancing Translational Sciences; 2004. 2004. 2019 May 1., Bethesda (MD).
[41] Strober W. Trypan blue exclusion test of cell viability. Curr Protoc Im 2015;111:A3.B.1–3. https://doi.org/10.1002/0471142735.ima03bs111.
[42] Schindelin J, Arganda-Carreras I, Frise E, Kaynig V, Longair M, Pietzsch T, et al. Fiji: an open-source platform for biological-image analysis. Nat Methods 2012;9:676–82. https://doi.org/10.1038/nmeth.2019.
[43] Giavarina D. Understanding Bland altman analysis. Biochem Med 2015;25:141–51. https://doi.org/10.1201/b16720-37.
[44] Caldwell AR. SimplyAgree: an R package and jamovi module for simplifying agreement and reliability analyses. J Open Source Softw 2022;7:4148. https://doi.org/10.21105/joss.04148.
[45] Vidal A, Mendieta Zerón H, Giacaman I, Camarillo Romero M, del S, López SP, Meza Trillo LE, et al. A simple mathematical model for wound closure evaluation. Journal of the American College of Clinical Wound Specialists 2015;7:40–9. https://doi.org/10.1016/j.jccw.2016.07.002.
[46] Di Trapani M, Bassi G, Ricciardi M, Fontana E, Bifari F, Pacelli L, et al. Comparative study of immune regulatory properties of stem cells derived from different tissues. Stem Cell Dev 2013;22:2990–3002. https://doi.org/10.1089/scd.2013.0204.
[47] Menard C, Pacelli L, Bassi G, Dulong J, Bifari F, Bezier I, et al. Clinical-grade mesenchymal stromal cells produced under various good manufacturing practice processes differ in their immunomodulatory properties: standardization of immune quality controls. Stem Cell Dev 2013;22:1789–801. https://doi.org/10.1089/scd.2012.0594.
[48] Adamo A, Brandi J, Caligola S, Delfino P, Bazzoni R, Carusone R, et al. Extracellular vesicles mediate mesenchymal stromal cell-dependent regulation of B cell PI3K-akt signaling pathway and actin cytoskeleton. Front Immunol 2019;10:446. https://doi.org/10.3389/fimmu.2019.00446.
[49] Wang J, Zhou Y, Donohoe E, Canning A, Moosavizadeh S, Ryan AE, et al. Immunomodulatory potential of cytokine-licensed human bone marrow-derived mesenchymal stromal cells correlates with potency marker expression profile. Stem Cell 2024. https://doi.org/10.1093/stmcls/sxae053.
[50] Araki-Sasaki K, Ohashi Y, Sasabe T, Hayashi K, Watanabe H, Tano Y, et al. An SV40-immortalized human corneal epithelial cell line and its characterization. Investig Ophthalmol Vis Sci 1995;36:614–21.
[51] Wilson SE. Bowman's layer in the cornea– structure and function and regeneration. Exp Eye Res 2020;195:1–16. https://doi.org/10.1016/j.exer.2020.108033.Bowman.
[52] Jiang Q-W, Kaili D, Freeman J, Lei C-Y, Geng B-C, Tan T, et al. Diabetes inhibits corneal epithelial cell migration and tight junction formation in mice and human via increasing ROS and impairing Akt signaling. Acta Pharmacol Sin 2019;40:1205–11. https://doi.org/10.1038/s41401-019-0223-y.
[53] Fowler SA. Wound healing in the corneal epithelium in diabetic and normal rats. Exp Eye Res 1980;31:167–79. https://doi.org/10.1016/0014-4835(80)90076-7.
[54] Zhang Y, Chen P, Di G, Qi X, Zhou Q, Gao H. Netrin-1 promotes diabetic corneal wound healing through molecular mechanisms mediated via the adenosine 2B receptor. Sci Rep 2018;8:5994. https://doi.org/10.1038/s41598-018-24506-9.
[55] Gao N, Yu F-S. Lack of elevated expression of TGFβ3 contributes to the delay of epithelial wound healing in diabetic corneas. Investig Ophthalmol Vis Sci 2024;65:35. https://doi.org/10.1167/iovs.65.3.35.
[56] Zhou Q, Yang L, Wang Q, Li Y, Wei C, Xie L. Mechanistic investigations of diabetic ocular surface diseases. Front Endocrinol 2022;13:1079541. https://doi.org/10.3389/fendo.2022.1079541.
[57] Shih KC, Lam KS-L, Tong L. A systematic review on the impact of diabetes mellitus on the ocular surface. Nutr Diabetes 2017;7:e251. https://doi.org/10.1038/nutd.2017.4.
[58] Ladea L, Zemba M, Calancea MI, Călțaru MV, Dragosloveanu CDM, Coroleucă R, et al. Corneal epithelial changes in diabetic patients: a review. Int J Mol Sci 2024;25. https://doi.org/10.3390/ijms25063471.
[59] Ueno H, Hattori T, Kumagai Y, Suzuki N, Ueno S, Takagi H. Alterations in the corneal nerve and stem/progenitor cells in diabetes: preventive effects of insulin-like growth factor-1 treatment. Internet J Endocrinol 2014;2014:312401. https://doi.org/10.1155/2014/312401.
[60] Bu Y, Shih KC, Kwok SS, Chan YK, Lo AC-Y, Chan TCY, et al. Experimental modeling of cornea wound healing in diabetes: clinical applications and beyond. BMJ Open Diabetes Res Care 2019;7:e000779. https://doi.org/10.1136/bmjdrc-2019-000779.
[61] Müller LJ, Pels L, Vrensen GF. Ultrastructural organization of human corneal nerves. Investig Ophthalmol Vis Sci 1996;37:476–88.
[62] Power BM, Van Heerden PV. The physiological changes associated with brain death–current concepts and implications for treatment of the brain dead organ

donor. Anaesth Intensive Care 1995;23:26–36. https://doi.org/10.1177/0310057X9502300107.
[63] Shemie SD, Dhanani S. The physiology of brain death and organ donor management. Pediatr Crit Care Med: Volume 1: Care of the Critically Ill or Injured Child 2014:497–518. https://doi.org/10.1007/978-1-4471-6362-6_38.
[64] Watts RP, Thom O, Fraser JF. Inflammatory signalling associated with brain dead organ donation: from brain injury to brain stem death and posttransplant ischaemia reperfusion injury. J Transplant 2013;2013:521369. https://doi.org/10.1155/2013/521369.
[65] Sandiumenge A, Bello I, Coll-Torres E, Gomez-Brey A, Franco-Jarava C, Miñambres E, et al. Systemic inflammation differences in brain-vs. Circulatory-dead donors: impact on lung transplant recipients. Transpl Int 2024;37:12512. https://doi.org/10.3389/ti.2024.12512.
[66] Gordon JK, McKinlay J. Physiological changes after brain stem death and management of the heart-beating donor. Cont Educ Anaesth Crit Care Pain 2012;12:225–9. https://doi.org/10.1093/bjaceaccp/mks026.
[67] Essien E-O, Fioretti K, Scalea TM, Stein DM. Physiologic features of brain death. Am Surg 2017;83:850–4. https://doi.org/10.1177/000313481708300835.
[68] Anwar ASMT, Lee J-M. Medical management of brain-dead organ donors. Acute and Critical Care 2019;34:14–29. https://doi.org/10.4266/acc.2019.00430.
[69] McKeown DW, Bonser RS, Kellum JA. Management of the heartbeating brain-dead organ donor. Br J Anaesth 2012;108(Suppl):i96–107. https://doi.org/10.1093/bja/aer351.
[70] Yu Z, Hao R, Du J, Wu X, Chen X, Zhang Y, et al. A human cornea-on-a-chip for the study of epithelial wound healing by extracellular vesicles. iScience 2022;25:104200. https://doi.org/10.1016/j.isci.2022.104200.
[71] Saccu G, Menchise V, Gai C, Bertolin M, Ferrari S, Giordano C, et al. Bone marrow mesenchymal stromal/stem cell-derived extracellular vesicles promote corneal wound repair by regulating inflammation and angiogenesis. Cells 2022;11. https://doi.org/10.3390/cells11233892.
[72] Tao H, Chen X, Cao H, Zheng L, Li Q, Zhang K, et al. Mesenchymal stem cell-derived extracellular vesicles for corneal wound repair. Stem Cell Int 2019;2019:5738510. https://doi.org/10.1155/2019/5738510.
[73] Pérez ML, Barreales S, Sabater-Cruz N, Martinez-Conesa EM, Vilarrodona A, Casaroli-Marano RP. Amniotic membrane extract eye drops: a new approach to severe ocular surface pathologies. Cell Tissue Bank 2022;23:473–81. https://doi.org/10.1007/s10561-021-09962-4.
[74] Vazirani J, Sridhar U, Gokhale N, Doddigarla VR, Sharma S, Basu S. Autologous serum eye drops in dry eye disease: preferred practice pattern guidelines. Indian J Ophthalmol 2023;71:1357–63. https://doi.org/10.4103/IJO.IJO_2756_22.
[75] Tahmaz V, Menghesha L, Stern ME, Holtick U, Scheid C, Steven P. Insulin eye drops for severe refractory chronic ocular graft-versus-host disease. Bone Marrow Transplant 2024;59:1031–3. https://doi.org/10.1038/s41409-024-02272-9.
[76] Sacchetti M, Lambiase A, Schmidl D, Schmetterer L, Ferrari M, Mantelli F, et al. Effect of recombinant human nerve growth factor eye drops in patients with dry eye: a phase IIa, open label, multiple-dose study. Br J Ophthalmol 2020;104:127–35. https://doi.org/10.1136/bjophthalmol-2018-312470.
[77] Kanu LN, Ciolino JB. Nerve growth factor as an ocular therapy: applications, challenges, and future directions. Semin Ophthalmol 2021;36:224–31. https://doi.org/10.1080/08820538.2021.1890793.
[78] Costa-Ferro ZSM, Rocha GV, da Silva KN, Paredes BD, Loiola EC, Silva JD, et al. GMP-compliant extracellular vesicles derived from umbilical cord mesenchymal stromal cells: manufacturing and pre-clinical evaluation in ARDS treatment. Cytotherapy 2024. https://doi.org/10.1016/j.jcyt.2024.04.074.
[79] Lau H-C, Han DW, Park J, Lehner E, Kals C, Arzt C, et al. GMP-compliant manufacturing of biologically active cell-derived vesicles produced by extrusion technology. Journal of Extracellular Biology 2022;1:e70. https://doi.org/10.1002/jex2.70.
[80] Syromiatnikova V, Prokopeva A, Gomzikova M. Methods of the large-scale production of extracellular vesicles. Int J Mol Sci 2022;23. https://doi.org/10.3390/ijms231810522.